REPORT NO.
UCB/SESM-86/02

STRUCTURAL ENGINEERING AND
STRUCTURAL MECHANICS

EFFECT OF CONDENSED SILICA FUME ON THE STEEL-CONCRETE BOND

by

ODD E. GJORV

PAULO J.M. MONTEIRO

and

P. KUMAR MEHTA

JANUARY 1986

DEPARTMENT OF CIVIL ENGINEERING
UNIVERSITY OF CALIFORNIA
BERKELEY, CALIFORNIA

Table of Contents

EFFECT OF CONDENSED SILICA FUME ON THE STEEL-CONCRETE BOND

ABSTRACT

The objective of the present work was to study the effect of condensed silica fume on the mechanical behavior of the steel-concrete bond, and further to provide more basic information in order to explain the observed effects.

The mechanical behavior was studied by using the pull-out test (ASTM C234) on concrete of varying compressive strength (5000-6000-9000-12000 psi) and varying contents of silica fume (0-8-16 % by weight of cement).

The effect of silica fume on the steel-cement paste transition zone was studied on small composite specimens by use of scanning elactron microscopy and X-ray diffraction analysis.

The mechanism of the reinforcing steel-concrete bond is rather complicated and there is a number of factors affecting the bond strength. On the basis of the experimental results presented in this report, however, the following conclusions appear to be warranted:

(1) Increased additions of condensed silica fume up to 16 percent by weight of cement showed an improving effect on the pull-out strength, especially in the high compressive strength range of the concrete.

(2) The presence of silica fume did affect the morphology and microstructure of the steel-cement paste transition zone. Thus both porosity and thickness of the transition zone were reduced.

(3) The observed effect of silica fume may be explained by the following mechanisms:

1. Less free water accumulated at the interface during the casting of the specimens.
2. Preferential orientation of CH crystals was considerably reduced.
3. Pozzolanic reaction between CH and condensed silica fume caused densification.

Acknowledgements

The present work was carried out when the first author was a Visiting Professor at the SESM Division during the academic year 1983-84. This author wishes to thank the financial support provided by the Royal Norwegian Council for Scientific and Industrial Research, Elken A/S Chemicals and A/S Hoyer Ellefsen. He also gratefully acknowledges the scholarship given by the Fullbright program.

The authors would like to thank Lou Tresconi and George Hayler for valuable assistance in the laboratory.

1. Introduction

Concrete is a composite material consisting of aggregate and cement paste, and reinforced concrete is a composite material consisting of concrete and reinforcing steel. For all composites the bond between the individual constituents is the most critical factor for the properties of the composite material. Provided good properties of the constituents any improvement of the bond will improve the properties of the composite material.

For a reinforced concrete composite the bond can be considered as the shearing stress between the concrete and the reinforcing bar (1). It is the result of adhesion, friction, and support of the ribs. Plain bars rely mainly on adhesion and friction, while deformed bars depend mainly on the support of the ribs. Strands derive their bond resistance from adhesion, friction, and a mechanism called "lack of fit" which occurs if the wires of a strand will not fit into the mark of the new position, resulting in a wedge action and more friction (2).

The importance of the bond between the reinforcing bar and concrete on cracking, deflection, and anchorage of steel in reinforced concrete has been realized for a long time. In 1913, Abrams (3) performed pull-out tests using plain bars to determine the effect of settlement and shrinkage of concrete on the bond. His experiments showed that bars cast in a horizontal position exhibited lower bond resistance than vertical bars. Later on, Menzel (4) established the fundamental importance of the depth of concrete under a horizontal bar. He showed that as the depth of concrete under the bar increased, the bleeding water accumulated under the bar also increased, thereby weakening the bond resistance. Also his experimental results showed that the best performance was observed for vertical bars pulled against the direction of casting. This topic was further studied by Clark (5,6), Collier (7), Jirsa et al. (8) among others, and the main conclusions were the following:

1. The bond of deformed bars is affected by the type of deformation, the position of anchorage, and the consistency of concrete. The bar size has little effect on the pattern of strength reduction with height

2. The bond ratio between the top-cast reinforcing bar and the bottom-cast bar decreases as the casting height increases

3. An increase in anchorage length does not produce a significance change in the bond efficiency of the top bar

4. An increase in slump reduces the bond capacity as the depth of concrete is increased

Initially research was concentrated on the global efficiency of the bond, and later it focused on the bond mechanisms, interface stresses, and relative displacements. The work of the following researchers should be mentioned: Mains (9), Bresler and Bertero (10), who measured the distribution of bond stress using electrical strain gages; Broms (11) who analyzed the relationship of bond slip and crack spacing; Lutz and Gergely (1) who studied the bond slip and bond splitting of deformed reinforced bars.

A great improvement in the modeling of the reinforcing concrete was achieved with the development of the finite element method, which permitted simulation of the effects of cracks in the reinforcing concrete by analyzing either sharp cracks or distributed cracks. The first condition of analysis, i.e., the sharp crack (12), can be implemented by doubling the nodes through which the crack propagates or by varying the stiffness of the linkage elements that connect the nodes of adjacent elements. One of the shortcomings of this approach is that the location and orientation of the cracks are not known in advance. As pointed out by Cedolin and Bazant (13), unless the nodes locations are considered as variables and unknown so that the nodes coordinates are redefined, the crack propagation will necessarily coincide with the original element boundaries. The alternative to the discrete cracks is the continuous smeared-cracking model. In this approach, concrete becomes orthotropic after the first cracking has occurred. It should be noted that cracking is treated as a change in the material properties and that this formulation easily allows the account of aggregate interlocking by retaining a positive shear modulus, which means that secondary cracking does not necessarily appears perpendicular to the first direction of the cracks (14).

The main restriction to the use of the traditional finite element method is the lack of a precise criterion for crack propagation. The usual procedure of comparing the stress state resulting from the analysis with the tensile strength of concrete may be misleading: for example with a sharp crack, the stress concentration may be increasingly higher as the mesh in front of the crack is refined, and this causes a lack of objectivity since the concrete may or may not crack depending on the size of the element grid in front of the crack. Since this limitation is related to the lack of criterion for crack propagation, a natural source of inspiration is the fracture mechanics approach. However, for a number of reasons, concrete researchers were reluctant to use fracture mechanics principles. What they questioned was the simple use of the linear fracture mechanics for such a heterogeneous material. Recently, a series of developments were obtained by means of the non-linear fracture mechanics, namely the J-integral (15), COD (15, 16), R-curve analysis (15,17,18) and the "fictitious" crack model (19,20,21), the last two being the most promising for concrete. Returning to the crack propagation criteria, Bazant and Cedolin (22,23,24) proposed the use of an energy criterion based on fracture mechanics. They showed that using this criterion, the results became independent of both the element size and the type of element used.

The characterization of the steel-cement paste interface morphology attracted less attention, and little effort was spent in trying to correlate the microstructure and the mechanical properties. One of the few exceptions is the work of Al Khalaf (25) and Morino (26) who studied the interface between mild steel and cement paste or mortar. Also the comprehensive work of Sakamoto and Iwasaki (27) in describing the influence of sodium chloride on the concrete-steel bond should be mentioned.

The transition zone between aggregate and cement paste has been analyzed by many researchers. Farran (28,29) observed that calcium hydroxide crystals would grow preferentially in the contact zone between cement paste and aggregate. Subsequently, Maso (30) set forth the hypothesis that there is a transition zone due to the different diffusion of ions in the cement paste near the aggregate. Hadley (31), using a scanning electron microscope and X-

ray spectrometer combination, was able to describe many interesting processes that occur at the interface. His experimental results made it possible to describe the sequence of formation of hydration products at the interface as follows: A layer of CH film is precipitated with the c-axis perpendicular to the aggregate surface and over this film, a CSH layer is formed, creating a composite or "duplex" film. This film will be bound to the bulk paste by the growth of large impure CH crystals as hydration process continues. Barnes (32) studied the morphology of the paste-aggregate interface using four different portland cements (including a portland blast furnace slag cement) and confirmed most of Hadley's conclusions. However, Struble and Mindess (33) reported that the layer of well-oriented calcium hydroxide crystals on the interface did not constitute a duplex film.

Iwasaki and Tomiyama (34) suggested the three following stages during the interface formation: precipitation of ettringite needles over the aggregate, precipitation of calcium hydroxide plates and densification of the contact film.

Parallel work done by French researchers showed the existence of an "auréole de transition" (35) around the aggregate. Perrin (36), using a transmission electron microscope showed that in the auréole the hydration crystals were different from the ones formed in the bulk cement paste. Grandet and Ollivier (37) were able to analyze the change in hydration products from the interface to the bulk cement paste by using X-ray diffraction, and adopting a process of successive abrasion of the interface.

In the present report the effect of condensed silica fume on the bond and interaction between concrete and steel has been studied both in a macroscopic and microscopic level.

2. Experimental

2.1 Materials

In order to study the mechanical behavior of the bond the pull-out strength at four levels of concrete compressive strength (3000, 6000, 9000 and 12000 psi) was investigated. For these strength levels three levels of condensed silica fume was used, 0, 8 and 16 percent by

weight of cement, respectively. The mix design of all these 12 mixes is shown in Table 1.

An ASTM Type I-II portland cement with the chemical analysis shown in Table 2 was used. The fine aggregate was a Kaiser Radum top sand with 2.68 bulk specific gravity, 0.9-percent absorption, and 2.93 fineness modulus. Two types of coarse aggregate were used, one crushed limestone and one quartz type of gravel with 2.69 and 2.63 bulk specific gravity respectively and approximately 0.5-percent absorption. For both aggregates the fineness modulus was 7.0. The fine and coarse aggregate had a gradation as ahown in Table 3.

Condensed silica fume with a particle size distribution as shown in Fig. 1 was used. About 82 and 36 percent of the material was finer than $1\nu\ m$ and $0.2\nu\ m$,respectively, with an average particle diameter of approximately $0.1\nu\ m$. The specific surface was in the range of 20-25 m^2/g. It consisted of 93 percent silica and had a density of 2.2 g/cm^3.

As a water-reducing admixture a lignosulfonate (ZeeCon R40) was used. The specific gravity of the material was 1.2 g/cm^3 with 42 percent solids.

For the pull-out tests twenty-four in. long plain and deformed #6 steel bars (19 mm) were used. The steel quality was A-36 with a minimum f_y of 60 Ksi.

For the microstructure characterization of the steel-cement paste transition zone a pure cement paste, with a water-cement ratio of 0.35 was used. For these tests three levels of silica fume was used, 0-5 and 16 percent by replacement, respectively. For the 16 percent silica fume replacement one percent of the lignosulfonate was also used. For some of the specimens with 16 percent replacement 2 percent calcium chloride (analytical reagent) by weight of cement was also added.

2.2 Testing Procedure

2.2.1 Pull-out testing

The concrete mixes were batched in a pan mixer with rotating blades. ASTM specifications were followed for the mixing, for the slump test and for the preparation of the specimens.

The pull-out testing was carried out according to ASTM C 234. For each concrete mix two double specimens with horizontal positions was cast. For each mix ten cylindrical specimens (4 by 8 in.) for compressive and splitting tests were also prepared.

It should be noted that all specimens for pull-out testing were made with limestone aggregate. Only for the compressive and splitting tests specimens of both limestone and quartz aggregate were prepared.

The specimens were kept in their molds for 24 hours and then stored in a fog room at 23 C. All tests were performed at the ages of 28 days.

2.2.2 Steel-cement paste transition zone

In order to study the interface as described by Grandet and Ollivier (37) composite specimens were used, consisting of cement paste cast against a polished steel surface. For the purpose of measuring accurately the thickness of the hydration products formed at the interface it was essential that the surface of the steel was polished down to one micron. At some specified ages, the specimen was broken at the interface of the two distinct materials (Fig. 2). The two halves obtained from the composite specimen were analyzed by a scanning electron microscope (SEM) attached to an energy dispersive analysis (EDAX) and by X-Ray diffraction (XRD).

The steel had a cylindrical form and a diameter of 3/4 in. A PVC tube with the same diameter was mounted on top of the polished face of the of the steel. RTV 108 Silicone Rubber was used as a cement and sealant device.

Cement paste was cast (with 0.35 w/c), and the composite specimen was covered with Saran wrap and stored in a fog room. At specified ages the specimens were removed from the fog room and placed in a dessicator with drierite for drying. Due to the drying shrinkage the cement paste and the aggregate separated at the interface.

Acetone was used to stop hydration. The specimens were then stored in a dessicator containing silica gel (55 % R.H.) and Ascarite (to avoid carbonation).

The specimens for the SEM analysis were coated with a layer of gold and stored in the dessicator containing silica gel and Ascarite.

For some of the specimens, the interface on the cement matrix side was analyzed by XRD, and then this surface was removed by abrasion and the new surface was reanalyzed. This iteration would stop when the results of XRD on consecutive surfaces was practically the same (Fig. 2). Silicon carbide papers (400 and 600 grit) were used as the abrasive medium for successive removal of material from the interface. This material was weighed in a balance with 0.1 mg precision, so by knowing its density the distance from the interface could be determined. It was assumed, however, that the density of the interface layers was the same as that of the bulk cement paste. This is not true since the density of the interface should be smaller. The lack of accurate density data for the interface layers does represent an inherent flaw of this process, which prevents it from being fully quantitative; however it does show important features when used for comparative purposes.

The morphology study was performed using a Hitachi Scanning Electron Microscope, model S-415 A, which had a magnification power up to 150,000 X. An X-ray detector was attached, and that allowed various scanning modes needed for elemental analysis.

The mineralogical composition of the interface was analyzed with a Rigaku X-ray diffraction equipment attached to a computer terminal.

3. Test Results and Discussions

3.1 Pull-out strength

The results of the compressive and tensile strength is shown in Table 4. As can be seen the compressive strength results for the limestone aggregate were close to the target strength levels, with the exception of the concrete mix with no silica fume that failed to get the aimed strength of 12,000 psi. The 9,000 psi concrete was also somewhat lower. The quartz aggregate did not give the same high compressive strength as the limestone aggregate. It should be noted, however, that for the higher strength levels, the quartz gave the highest tensile strength.

For the limestone aggregate the tensile-to-compressive strength ratio was approximately 0.14 for the lower strength of the limestone concrete (for all the three levels of silica fume), and it was reduced to 0.08 for the higher strength concrete. This decrease is typical, and the interesting point is that the ratio was not very dependent on the level of silica fume for a given compressive strength level.

The results of the pull-out tests are summarized in Tables 5, 6 and 7. These results show the major influence of the bar position on the bond strength, the "upper" bars showing in most cases a lower strength because they had much higher concrete bleeding which resulted in the accumulation of water and air beneath the lugs with consequent loss of bond strength. For plain bars, as the concrete strength increases the difference of the two bars tends to decrease because the higher amount of cementitious material that is used tends to diminish the concrete bleeding, thus producing a more uniform material.

For lower loads, chemical adhesion associated with mechanical interaction prevents slip. When adhesion is lost and consequently slip occurs, the ribs of a deformed bar will restrain this movement. Lutz and Gergely (1) proposed that slip of a deformed bar can occur in two ways: (a) the ribs can push the concrete away from the bar by a wedging action, and (b) the ribs can crush the concrete. They showed also that ribs with a face angle between 40° and 105° produce approximately the same movement. For these ribs, slip is produced mainly due to the crushing of the concrete in front of the rib, once the existing friction between the face of the rib and the concrete is enough to avoid relative movement at the interface. As concrete is being crushed, it is lodged in front of the rib in such a way as to produce an effective face of the rib with angles of 30° and 40° (Fig. 3).

Goto (39,40) experimentally investigated the bond mechanism by injecting ink into the loaded specimen. After the test, the specimen was split in half along planes that included the bar axes. By this process, it was possible to analyze the internal cracks existing in the concrete. Goto observed that when deformed bars were used lateral cracks ("primary cracks") were formed; and also around the deformed bars just after the formation of primary cracks

small internal cracks developed which did not appear at the concrete surface. When the steel stress became high, new lateral cracks ("secondary cracks") formed near the primary cracks. This caused the development of large hoop stresses in the concrete close to the bar, resulting in possible localized longitudinal cracks. Tepfers (38,41) analyzed the condition in which the splitting cracks spread across the whole concrete cover of the bar. He considered that the radial components of the bond forces are balanced against "concrete rings" in tension, which resist the tensile hoop stresses as shown in Fig. 4.

A typical failure mode of a pull-out specimen using a deformed bar is shown in Fig. 5. A detail of the fractured specimen is shown in Fig. 6. Thus, the pull-out strength for the deformed bars was also affected by the tensile strength of the concrete.

Fig. 7 shows the graph of the pull-out strength versus the concrete compressive strength for each bar. The results were fitted with the expression $f_{pull-out} = K_1 f_c^{K_2}$, where $f_{pull-out}$ is the pull-out strength, f_c the concrete compressive strength, and K_1 , K_2 are constants. The results for plain bar with the concrete mix 0-6000 were not included in the regression because they were not reliable. As can be seen and has been reported before, the concrete compressive strength plays a major role in the pull-out strength. The presence of silica fume did also have an effect on the pull-out strength, especially in the high compressive strength range of the concrete.

Figs. 8A and B show isometric projections for the pull-out strength as a function of the compressive strength of concrete and the amount of silica fume. The projections were obtained from interpolation of the results and not from a mathematical expression. It can be seen that the surface increases as the compressive strength or the amount of silica fume increases.

The dependence of the pull-out strength on the tensile and compressive strength of concrete is shown in the isometric projections of Figs. 9A and B.

As already discussed the mechanism of the reinforcing steel-concrete bond is rather complicated. From the above test results, however, it appears that the presence of silica fume

improves the bond. In order to explain this effect it was natural to look into the effect of silica fume on the morphology and microstructure of the steel-cement paste transition zone

3.2 Morphology of the steel-cement paste transition zone

When cement paste is cast against a steel surface, a transition zone with a high water-cement ratio is produced. As previously discussed, in this transition zone calcium hydroxide (CH) crystals with the c-axis perpendicular to the interface is formed. Figs. 10 and 11 show the CH film (cement paste side) in a 30 days old specimen without silica fume. The CH film is smooth and even though the crystal structure behind it is dense, there is not a perfect union between the interfacial film and the transition zone.

For a specimen that contained 16 percent silica fume replacement at the same age (30 days) it is interesting to note that the global formation of CH film did not alter. Figs. 12 and 13 show, however, that the CH film is partly covered with CSH due to the pozzolanic reaction between the calcium hydroxide and the silica fume. It can also be seen that the CH film is united to the matrix by a dense interlocking. The pozzolanic reaction happens in localized zones and seems to introduce "welding points" on the steel-cement paste interface. However, the dominant effect that happens throught the specimen is the densification of the structure behind the film (Figs. 14 and 15). This causes a reduction of porosity in the transition zone which may explain the observed effect of silica fume on the bond strength.

Figs. 16 and 17 show the distribution of silica fume particles on the steel surface. It can be seen that they are partially reacted. Some silica fume particles react quickly during the early stages of hydration while others are only partially dissolved when an equilibrium is reached. Some of them may react later on with CH, , forming CSH on top of the film (Fig. 18 and 19). However, some silica fume particles, or their pseudomorphs, get engulfed in the CH film. The effect of these particles on the mechanical behavior of the film is not known, although it might be expected that these particles will reinforce the film. Figs. 20 and 21 show silica particles around a crack in the film (probably due to shrinkage). It can be seen

that the particles are fairly well distributed in the film and that they bridge the crack in various points. This process consumes energy, therefore these particles toughen the film. However, it should be noted that this is a local toughening effect; the global toughness of the specimen will depend on a variety of other factors such as the size of the flaws, the microstructure of the crystals, etc. Figs. 22A and 22B show other cracks in the interfacial film with low and high magnifications. Note the "kink" of the crack path due to the presence of one of these inclusions.

3.3 XRD Analysis of the Transition Zone

The method of successive abrasion of the interface and its analysis by XRD permits the characterization of the hydration products over the transition zone. Once the CH crystals are precipitated in a preferential orientation, it is not possible to perform a quantitative analysis of them with this method. It is convenient, therefore, to define an index of preferential orientation. Since the CH crystals tend to grow parallel to the steel surface, the (00.1) is a natural plane to select. The other plane chosen is (10.1), because there is not much interference with peaks of other hydration products.

$$R = \frac{I(00.1)}{I(10.1)}$$

The ratio R is 0.74 for random orientation of calcium hydroxide. Therefore, if it is desirable to know how much the orientation deviates from the random one, a ratio I can be used, defined as:

$$I = \frac{R}{0.74}$$

On the basis of this definition I is 1 for a random orientation and approaches infinity for a perfect orientation (c-axis). The ettringite is not subjected to preferential orientation, and its peak at 9.1° 2Θ ($Cu-K\alpha$) was selected because it is not interfered with by other peaks. Therefore it is possible to estimate the ettringite concentration over the transition zone.

The XRD method permits the analysis of the transition zone in a global way, while the

SEM only permits a localized analysis. When the composite specimen is fractured, some of the interfacial film (and some hydration products bonded to it) may adhere to the steel side, so that the thickness of the attached film is difficult to access. This creats a problem in defining the reference plane of the original interface. This uncertainity is particularly important for analysis closer to the interface since as already shown, the surface effect produced by the steel decreases exponentially with the distance from the interface. Therefore in fitting the data, in addition to the traditional method of the least squares, two other linear models, one minimizing the sum of the absolute residuals and the other using a robust criterion, were used in a system for interactive data analysis. It should be mentioned that the term "robustness" means relative insensitivity to moderate departures from assumptions.

The method of robust regression is used to analyze the behavior of least squares estimation when the disturbances are not well behaved. Coleman et al. (42) developed the computational procedures for iteratively reweighted least squares. Consider the vector of observations b (mx1), the data matrix A (mxn), the vector of parameters x (nx1) and a vector r (mx1) to model the equation b = Ax + 1. The least square solution consists in obtaining the minimum of $\sum_{i=1}^{m}((r_i(x))/s)^2$, where r is the residual vector of b-Ax and s is a constant.

The weighted least square approach consists in finding the minimum of $\sum_{i=1}^{m} W_{ii}((r_i(x))/s)^2$, where W is a diagonal matrix of weights that are functions of scaled residuals. In the case of iteratively reweighted least squares, an optimization exists in the sense that a function of scaled residuals is minimized. This function determines the formula for the weight function used. The other method consists in solving the linear l_1 data fitting problem. The motivation for using the l_1 approximation rather than the l_2 (least squares) approximation or an $l\infty$ approximation is that the first one is recommended for data that may contain inaccurate points compared to the overall accuracy of the data. The solution proposed by Barrodate and Roberts (43) was used for this method.

Tables 8 and 9 show the thickness and the orientation of the transition zone as affected by age and amount of silica fume.

The analysis of the results should be made with special care. It should be noted that the results only reflect a partial description of the morphology of the transition zone, and any hasty generalization of the microstructure description in the transition zone and even worse direct correlation of it to the mechanical properties will be bound to failure or incorrect predictions. One example would be the variation of the transition zone thickness with time. For a pure portland cement paste the thickness of the transition zone increases with time while the strength also increases with time, which may be a paradox. However, this paradox is eliminated when it is understood that the physical meaning of the transition zone thickness only is a measure of how far the surface effects produced by the steel surface will influence the bulk matrix.

The use of silica fume produces a remarkable decrease of the transition zone thickness as shown in Table 8 and Figs. 23A and B. The studies of Kurdowski and Nocun-Wczelik (44) showed that active silica powder accelerates the reaction of tricalcium silicate with water. Increasing additions of silica cause the development of greater heat and a shorter dormant period. It was concluded that the C_3S hydration is controlled by the conditions governing the liquid phase and that the reaction rate is controlled by the transportation process of calcium ions from the grain surface to the solution. In this case, C_3S hydration will be controlled by the consumption of Ca^{2+} ions from the solution as a result of the CH and CSH precipitation. Therefore the presence of a highly reactive silica lowers the calcium ions concentration in the solution forming CSH with low C/S ratio and increases the rate of C_3S hydration. Since the Ca^{2+} ions cannot easily diffuse in great quantity towards the steel surface, the preferential orientation of the CH crystals is decreased, and due to less accumulation of free water and due to the pozzolanic reaction the porosity in the transition zone is remarkably decreased.

Fig. 24 shows that there is a great concentration of ettringite near the aggregate surface

for all ages and all levels of silica fume. This observation supports the through-solution mechanism of cement hydration as the cement particles must dissolve to provide the calcium, sulfate, and aluminate ions to diffuse towards the steel surface where more ettringite get precipitated. It should be noted that the different levels of silica fume did not significantly influence the distribution of ettringite in the transition zone.

4. Conclusions

The mechanism of the reinforcing steel-concrete bond is rather complicated and there is a number of factors affecting the bond strength. On the basis of the experimental results presented in the present report, however, the following conclusions appear to be warranted.

(1) Increasing additions of condensed silica fume up to 16 percent by weight of cement showed an improving effect on the pull-out strength, especially in the high compressive strength range of the concrete.

(2) The presence of silica fume did affect the morphology and microstructure of the steel-cement paste transition zone. Thus both porosity and thickness of the transition zone were reduced.

(3) The observed effect of silica fume may be explained by the following mechanisms:

1. Less free water accumulated at the interface during the casting of the specimens.
2. Preferential orientation of CH crystals was considerably reduced.
3. Pozzolanic reaction between CH and CSF caused densification.

REFERENCES

1. Lutz L.A. and Gergely P., "Mechanics of Bond and Slip of Deformed Bars in Concrete". Journal of the American Concrete Institute, 64 , 711, 1967.

2. Vos E. and Reinhardt H.W., "Bond Stress-Slip Behavior of Deformed Bars, Plain Bars and Strands under Impact Loadings". *Bond in Concrete.* Ed. P. Bartos, Applied Science Publishers, London, 1982.

3. Abrams D.A., "Tests of Bond Between Concrete and Steel". Bulletin 71, Engineering Experimental Station, University of Illinois, 1973.

4. Menzel, C.A., "Some Factors Influencing Results of Pull-Out Bond Tests". Journal of the American Concrete Institute, 43 , No. 4, 1946.

5. Clark, A.P., "Bond of Concrete Reinforcing Bars". Journal of the American Concrete Institute, 46 , No. 3, 1949.

6. Clark A.P., "Comparative Bond Efficiency of Deformed Concrete Reinforcement Bars". Journal of the American Concrete Institute, 43 , No. 4, 1946.

7. Collier S.T., "Bond Characteristics of Commercial and Prepared Reinforcing Bars". Journal of the American Concrete Institute, 43 , 1947.

8. Jirsa J.O., Breen J.E., Luke J.J. and Hammad, "Effect of Casting Position on Bond". *Bond in Concrete.* Ed. P. Bartos, Applied Science Publishers, London, 1982.

9. Mains R.M., "Measurement of the Distribution of Tensile and Bond Stresses along Reinforcing Bars". Journal of the American Concrete Institute, 48 , 335, 1951.

10. Bresler B. and Bertero V.V., "Behavior of Reinforced Concrete Under Repeated Load". Trans. ASCE, J. Struct. Div., 94 , 1567, 1968.

11. Broms B. B., "Stress Distribution in Reinforced Concrete Members with Tension Cracks". Journal of the American Concrete Institute, 62 , N0. 9, 1095, 1965.

12. Ngo D. and Scordelis A.C., "Finite Element Analysis of Reinforced Concrete Beams". Journal of the American Concrete Institute, 64 , 711, 1967.

13. Cedolin L. and Bazant Z.P., "Fracture Mechanics of Crack Bands in Concrete". *Fracture Mechanics Methods for Ceramics, Rocks, and Concrete.* ASTM STP 745, S.W. Freiman and E.R. Fuller, Eds., American Society for Testing and Materials, 221, 1981.

14. Chen W.F., *Plasticity in Reinforced Concrete.* McGraw-Hill Book Co. Inc. New York, NY., 1982.

15. Velasco F., Visalvanich K. and Shah S.P., "Fracture Behavior and Analysis of Fibre Reinforced Concrete Beams". Cement and Concrete Research, 10 , 41, 1980.

16. Vesalvanich K. and Naaman A.E., "Evaluation of Fracture Techniques in Cementitious Composites". Journal of the Engineering Mechanics Division, ASCE, 107 , 1155, 1981.

17. Sek C., Baron J. and Francois D., "Mechanique de la Rupture Appliquee au Beton Hydraulic". Cement and Concrete Research, 9 , 641, 1979.

18. Wecharatana M. and Shah S.P., "Resistance to Crack Growth in Portland Cement Composites". *Fracture in Concrete.* edited by W.F. Chen and E.C. Ting, American Society of Civil Engineers, New York, 82, 1980.

19. Hillerborg A., Modees M. and Petersson P.E., "Analysis of Crack Formation and Crack Growth in Concrete by Means of Fracture Mechanics and Finite Elements". Cement and Concrete Research, 6 , 773, 1976.

20. Hillerborg A. "Analysis of Fracture by Means of the Fictitious Crack Model, Particularly for Fibre Reinforced Concrete". International Journal of Cement Composites, 2 , 177, 1980.

21. Petersson P.E., "Crack Growth and Development of Fracture Zones in Plain Concrete and Similar Materials". Ph.D. Thesis, Lund Institute of Technology, Sweden, 1981.

22. Bazant Z.P. and Cedolin L., "Fracture Mechanics of Reinforced Concrete". Journal of the Engineering Mechanics Division, Proceedings, American Society of Concrete Engineers, 106 , No. EM6, paper 15917, 1287, 1980.

23. Cedolin L. and Bazant Z.P., "Effect of Finite Element Choice in Blunt Crack Band Analysis". Computer Methods in Applied Mechanics and Engineering, 24 , 305, 1980.

24. Bazant Z.P. in Journal of Engineering Mechanics Division; Proceedings, American Society of Concrete Engineers, 102 , No. EM2, Proceedings, Paper 12042, , 331, 1976

25. Al Khalaf M.N., Page C.L., "Steel/Mortar Interfaces: Microstructural Features and Mode of Failure". Cement and Concrete Research, 9 , 197, 1979.

26. Morino K., "Properties of Bond Between Various Types of Rock Aggregate and Cement Paste". Transactions of the Japan Concrete Institute, 2 , 1980.

27. Sakamoto N. and Iwasaki N., "Influence of Sodium Chloride on the Concrete-Steel and Galvanized Steel Bond". *Bond in Concrete.* Ed. P. Bartos, Applied Science Publishers, London, 1982.

28. Farran J., "Contribution Minéralogique a l'Etude de l'Adhérence entre les Constituants Hydratés des Ciments et les Matériaux Enrobés". Revue Mater. Constr. Trav. Publ. 490,491,492 , 1956.

29. Farran J. and Maso J.C., Revue Mater. Constr. 587-588 , 1964.

30. Maso J.C., "La Nature Minéralogique des Agrégats, Facteur Essentiel de la Résistance des Bétons à la Rupture et à l'Action du Gel". Thèse, Toulouse , 1967.

31. Hadley D.H., "The Nature of the Paste-Aggregate Interface". Ph.D. Thesis. Purdue University, 1972.

32. Barnes B.D., "Morphology of the Paste-Aggregate Interface". Ph.D Thesis, Purdue University, 1975.

33. Struble L. and Mindess S., "Morphology of the Cement-Aggregate Bond". The International Journal of Cement Composites and Lightweight Concrete, 5 , 79, 1983.

34. Iwasaki N. and Tomiyama, "Bond Strength Between Cement Paste and Aggregate". Rev. 28th. Gen. Mtg., Cem. Assoc. Japan, 122 , 1974.

35. Farran J., Javelas R., Maso J.C. and Perrin B., "Existence d'une Auréole de Transition entre les Granulats d'un Mortier ou d'un Béton et la Masse de la Pâte de Ciment Hydraté". Comptes rendus 275 , 1467 , 1972.

36. Perrin B. "Observation en Microscopie Electronique des Caractères Morphologiques de la Liaison Pâte de Ciment Durci-Materiaux Enrobés". Ph.D Thesis, Toulouse, 1974.

37. Grandet J. and Ollivier J.P., "Nouvelle Méhtod d'Etude des Interfaces Ciment-Granulats". 7th International Congress on the Chemistry of Cement, Volume III, VII-85, Paris, 1980.

38. Tepfers R., "Cracking of Concrete Cover Along Anchored Deformed Bars". Magazine of Concrete Research, 31 , No. 106, 3, 1977.

39. Goto Y., "Cracks Formed in Concrete around Deformed Tension Bars". Journal of the American Concrete Institute, Proceedings, 68 , No. 4, 244, 1971.

40. Goto Y. and Otsuka K., "Experimental Studies on Cracks Formed in Concrete Around Deformed Tension Bars". The Technology Reports of the Tohoku University, 44 , No. 1, 49, 1979.

41 Tefpers R., "Tensile Lap Splices with Confining Reinforcement". *Bond in Concrete.* Ed. P. Bartos, Applied Science Publishers, London, 1982.

42. Coleman D., Holland P., Kaden N., Klena V. and Peters S.C., "A System Of Subroutines for Iteratively Reweighted Least Squares Computations". ACM Transactions on Mathematical Software, 6 , No. 3, 327, 1980.

43. Barrodale I. and Roberts F.D.K., "Solution of an Overdetermined System of Equations in the l_1 Norm". Communications of the ACM, 17 , No. 6, 1974.

44. Kurdowski W. and Nocun-Wczelik, "The Tricalcium Silicate Hydration in the Presence of Active Silica". Cement and Concrete Research, 13 , 341, 1983.

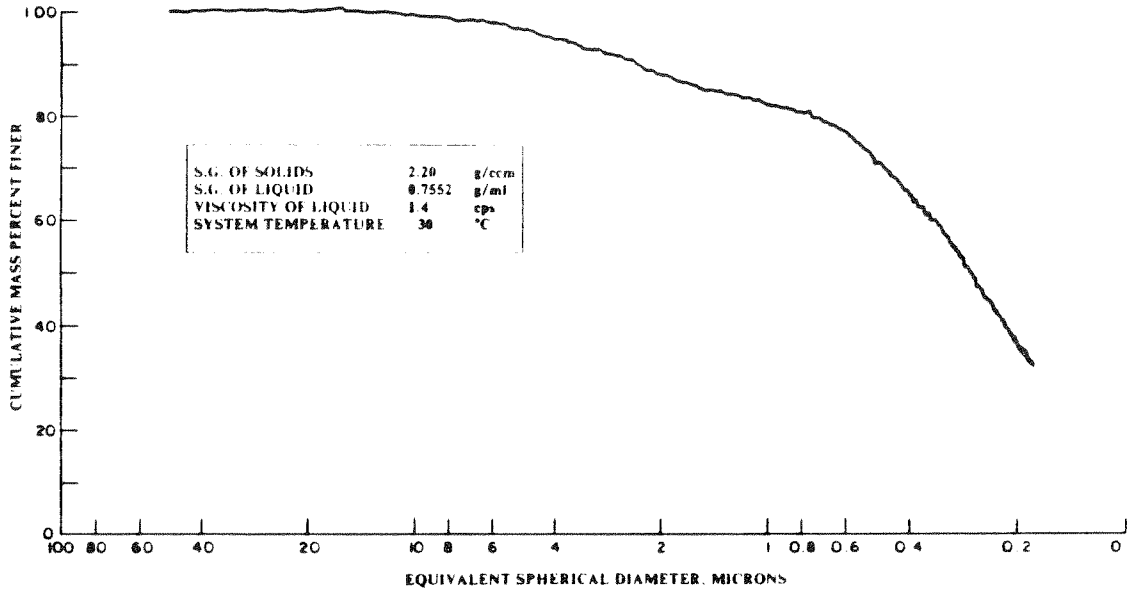

Fig. 1. Particle Size Distribution of Microsilica By X-Ray Sedimentation

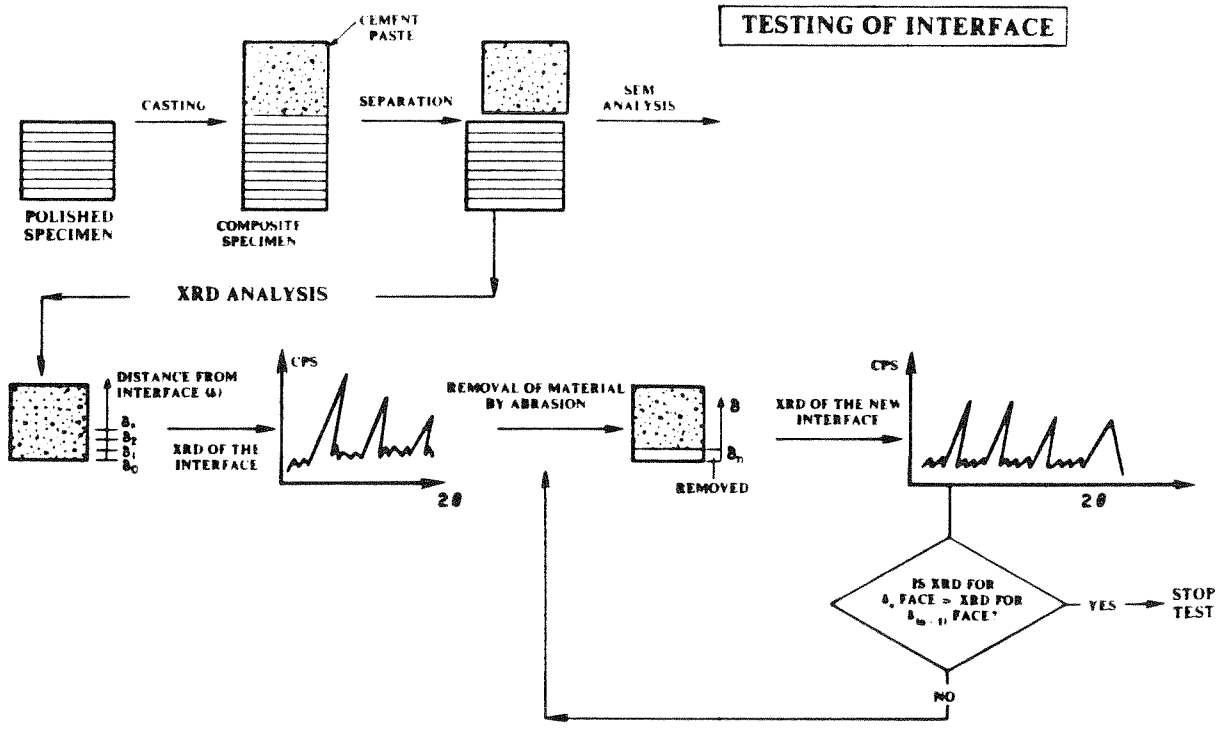

Fig. 2. Testing of Steel-Cement Paste Interface

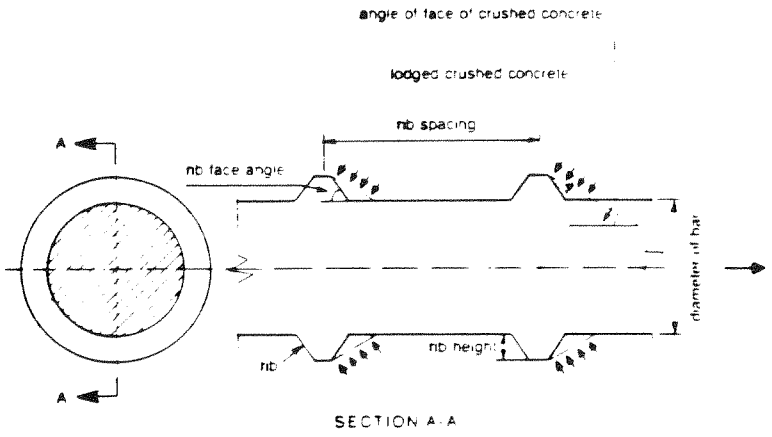

Fig. 3. The Geometry of a Deformed Reinforcing Bar and the Mechanical Interaction Between the Bar and the Concrete (38)

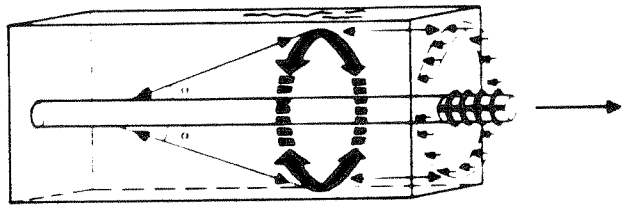

Fig. 4. Schematic Representation of How the Radial Components of the Bond Forces are Balanced Against Tensile Stress Rings in the Concrete in an Anchorage Zone (38)

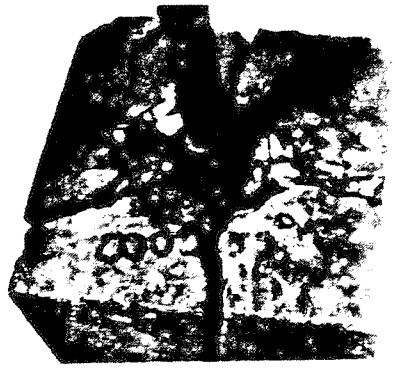

Fig. 5. Failure Mode of the Pull-Out Specimen with Deformed Bar

Fig. 6. Detail of the Fractured Specimen

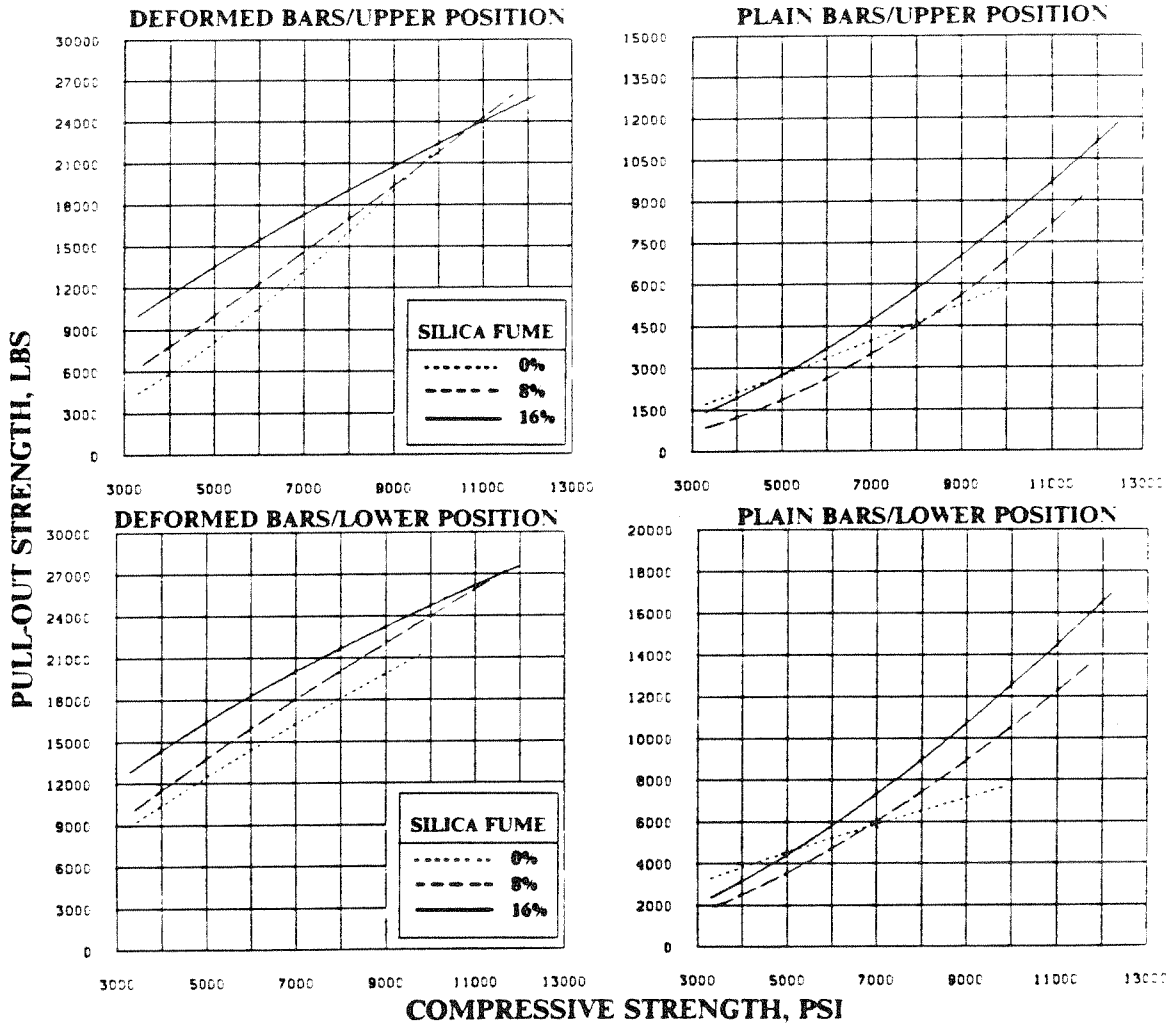

Fig. 7. Pull-Out Strength vs. Concrete Compressive Strength

DEFORMED BARS/Upper Position

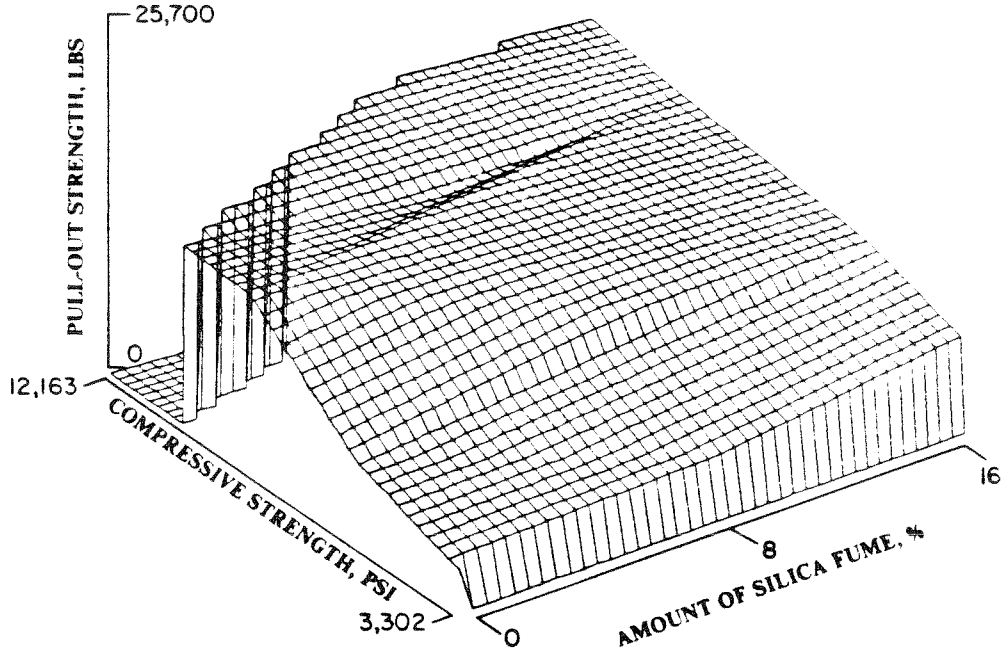

DEFORMED BARS/Lower Position

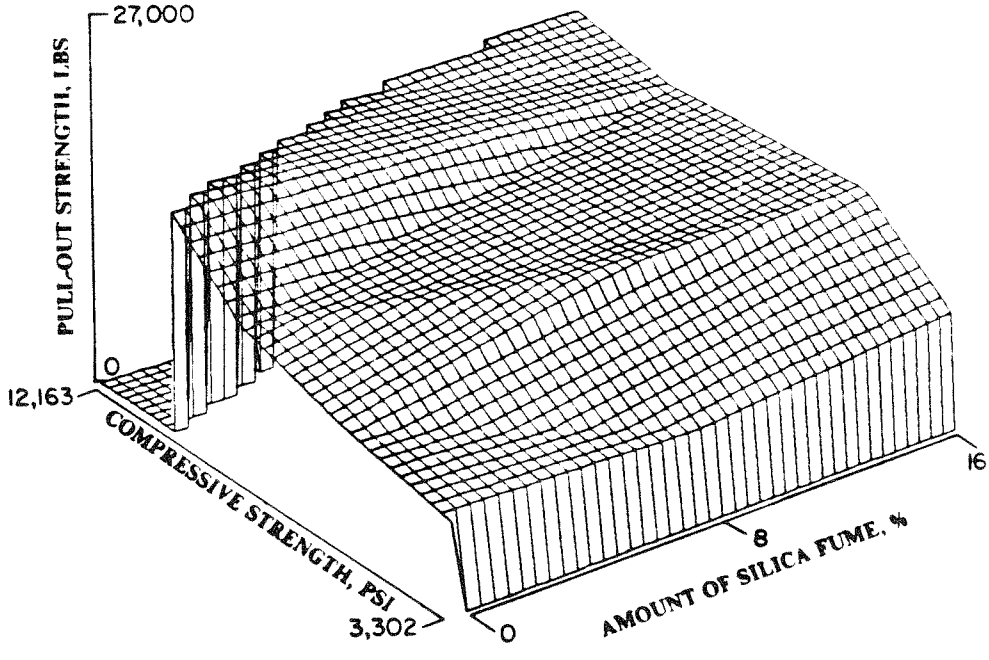

Fig. 8A. Pull-Out Strength in Function of the Concrete Compressive Strenth and the Amount of Silica Fume

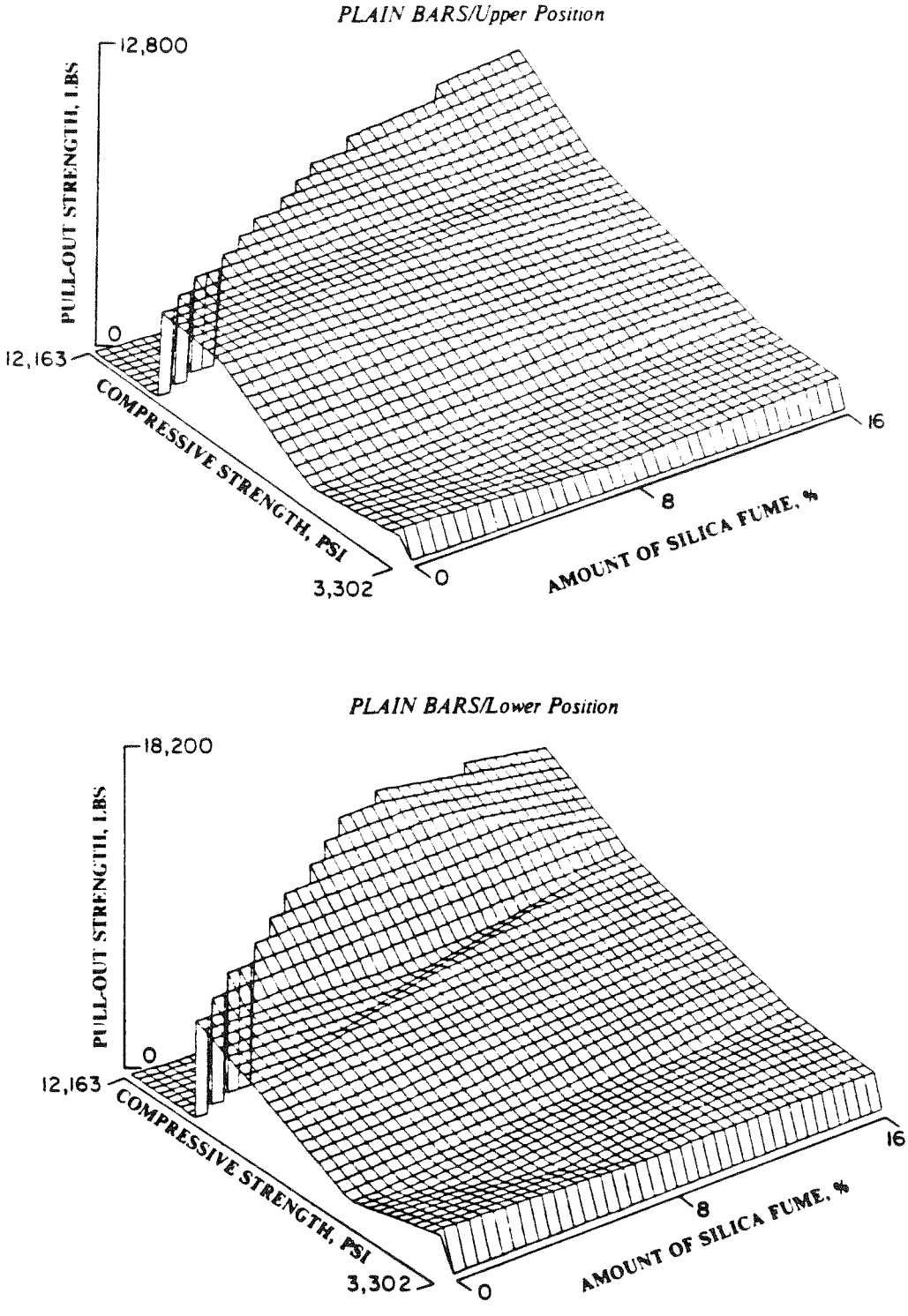

Fig. 8B. Pull-Out Strength in Function of the Concrete Compressive Strength and the Amount of Silica Fume

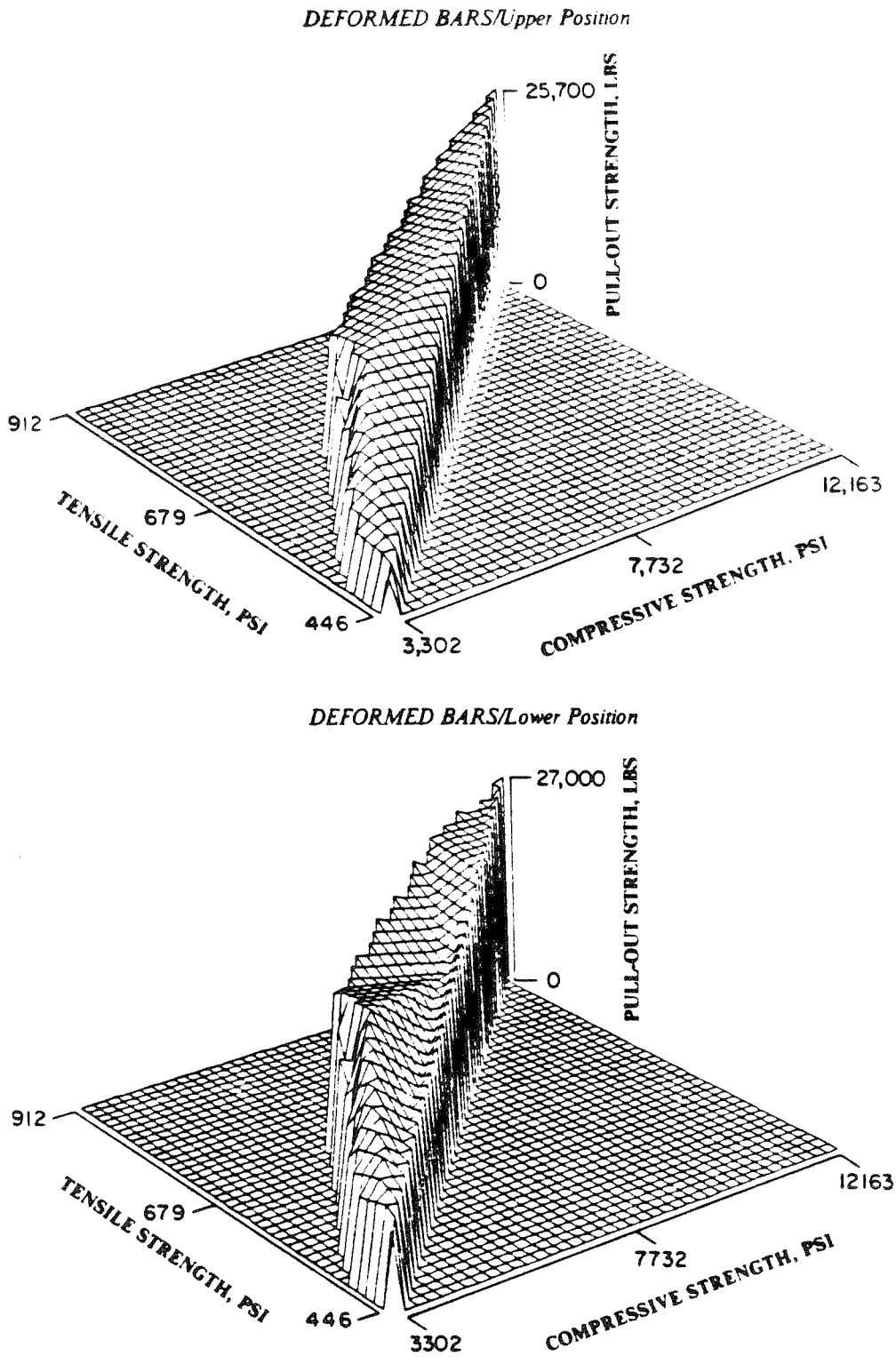

Fig. 9A. Pull-Out Strength in Function of the Tensile And Compressive Strength of Concrete

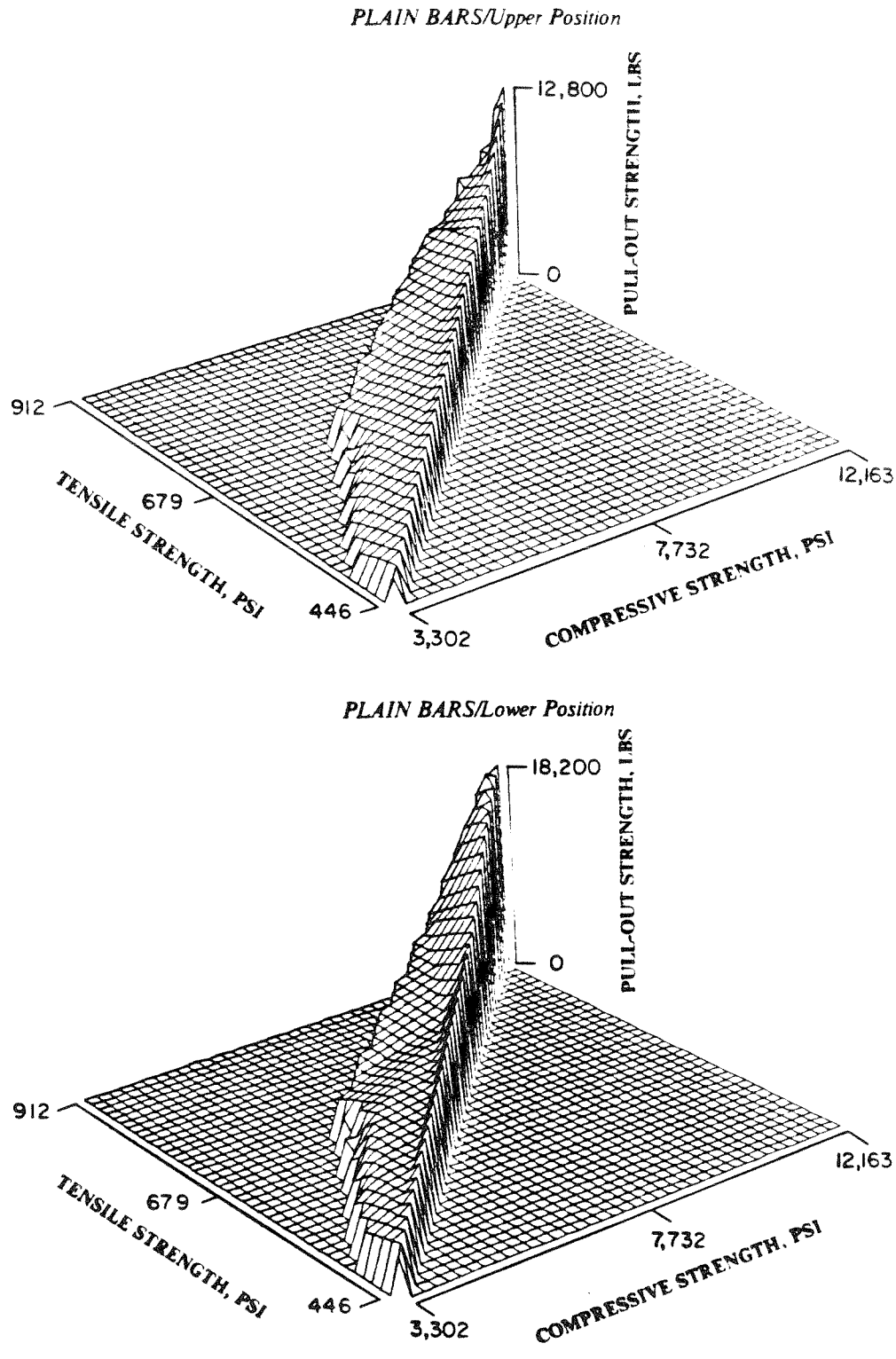

Fig. 9B. Pull-Out Strength in Function of the Tensile and Compressive Strength of Concrete

FIG. 10.
Calcium Hydroxide Film on the Cement Paste Side

FIG. 11.
Calcium Hydroxide Film on the Cement Paste Side (30 Days Old Specimen, No Silica Fume)

FIG. 12.
Pozzolanic Reaction on the Top of Calcium Hydroxide Film (30 Days Old Specimen, 16% Silica Fume)

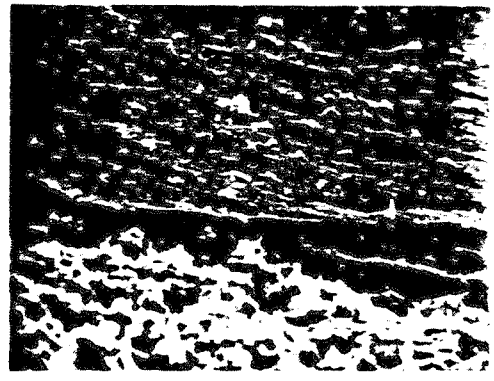

FIG. 13.
Densification of the Structure Behind the Calcium Hydroxide Film (30 Days Old Specimen, 16% Silica Fume)

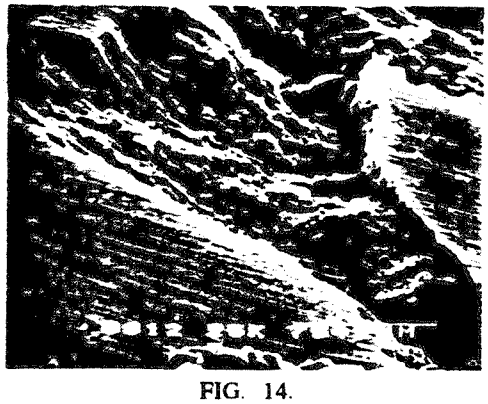

FIG. 14.
Another View of the Good Bond Between the Calcium Hydroxide Film and the Matrix When Silica Fume is Used

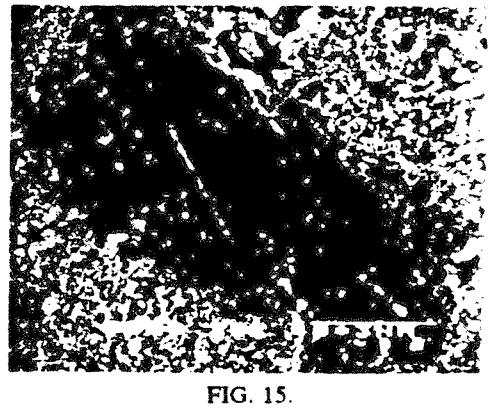

FIG. 15.
Calcium Hydroxide Film Surrounded by a dense Matrix (16% Silica Fume)

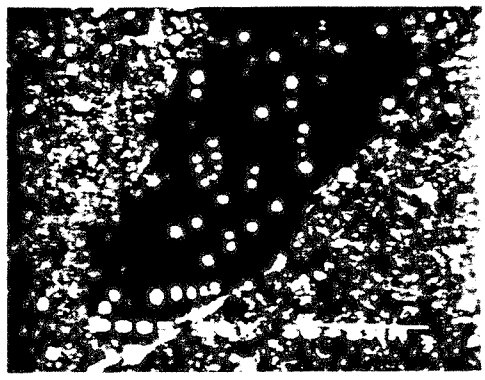

FIG. 16.
Distribution of Silica Fume Particles on the Steel Surface

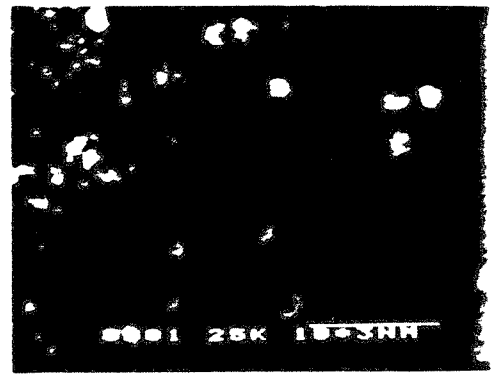

FIG. 17.
Detail of the Partially Dissolved Particles of Silica Fume on the Interface

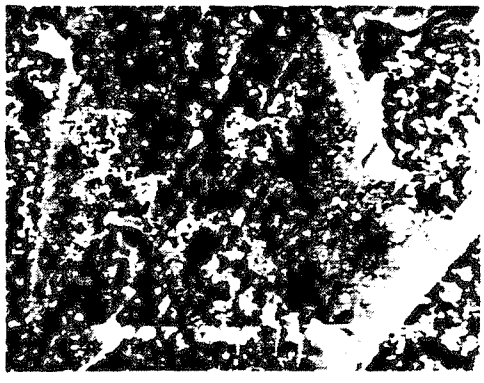

FIG. 18.
Pozzolanic Reaction on the Calcium Hydroxide Film

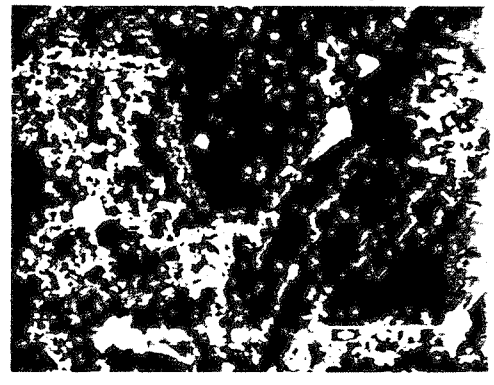

FIG. 19
Detail of the Pozzolanic Reaction

FIG. 20.
Silica Fume Particles Embedded on the Calcium Hydroxide Film

FIG. 21.
Silica Fume Bridging a Crack in the Calcium Hydroxide Film

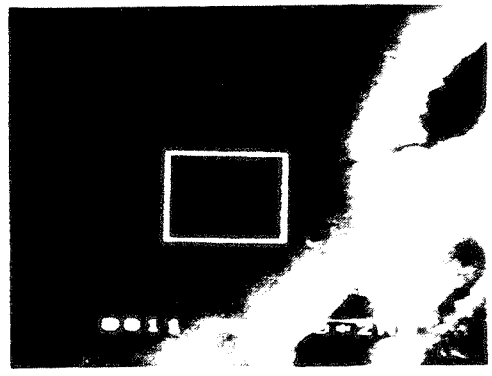

FIG. 22(A).
General Aspect of the Silica Fume Particles Dispersed in the Calcium Hydroxide Film

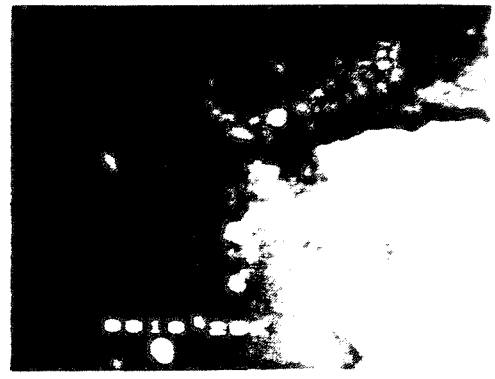

FIG. 22(B).
Detail of the Zone Delimited by the White Rectangle in Fig. 22(A)

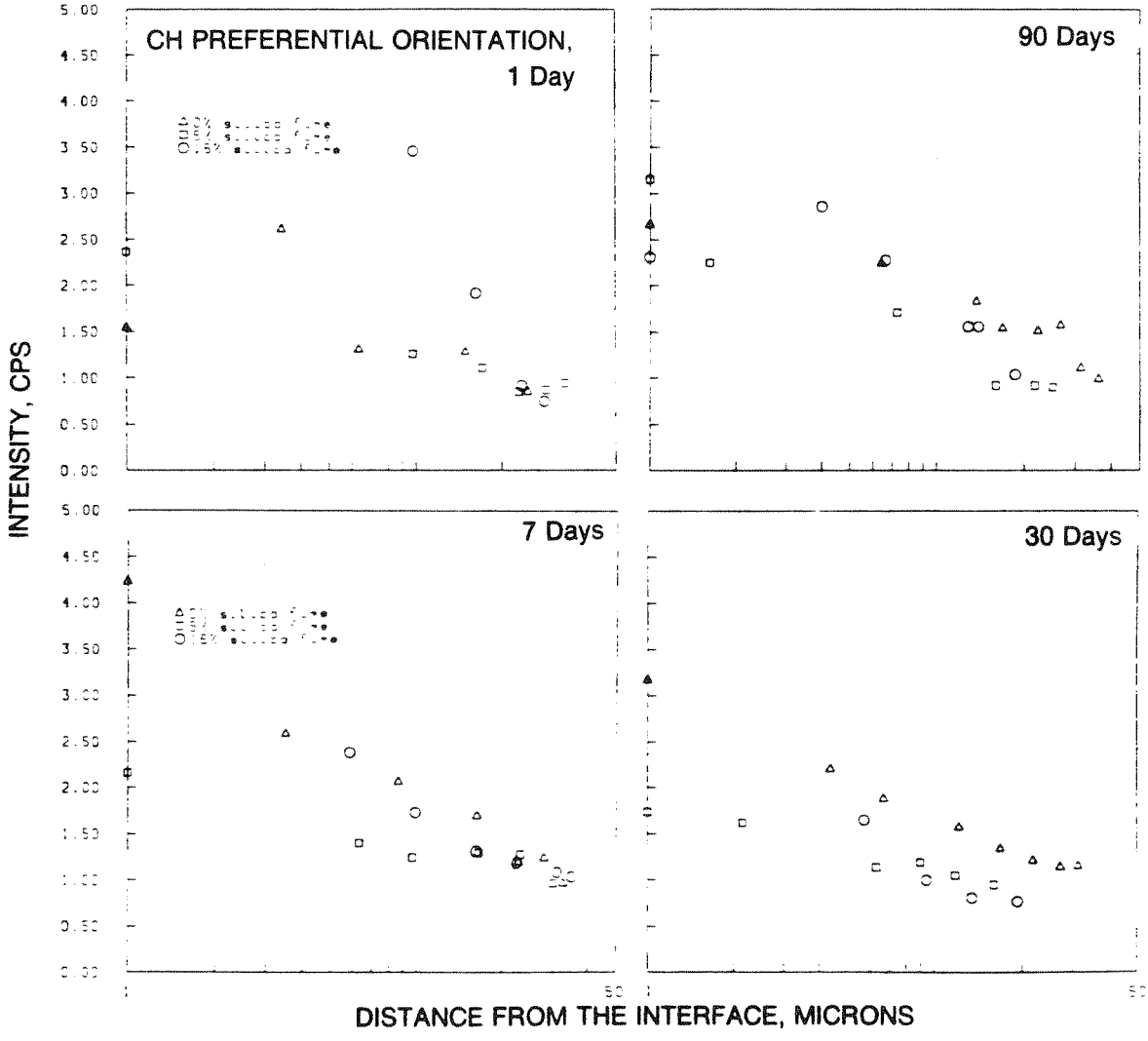

FIG. 23(A). Calcium Hydroxide Preferential Orientation in the Transition Zone

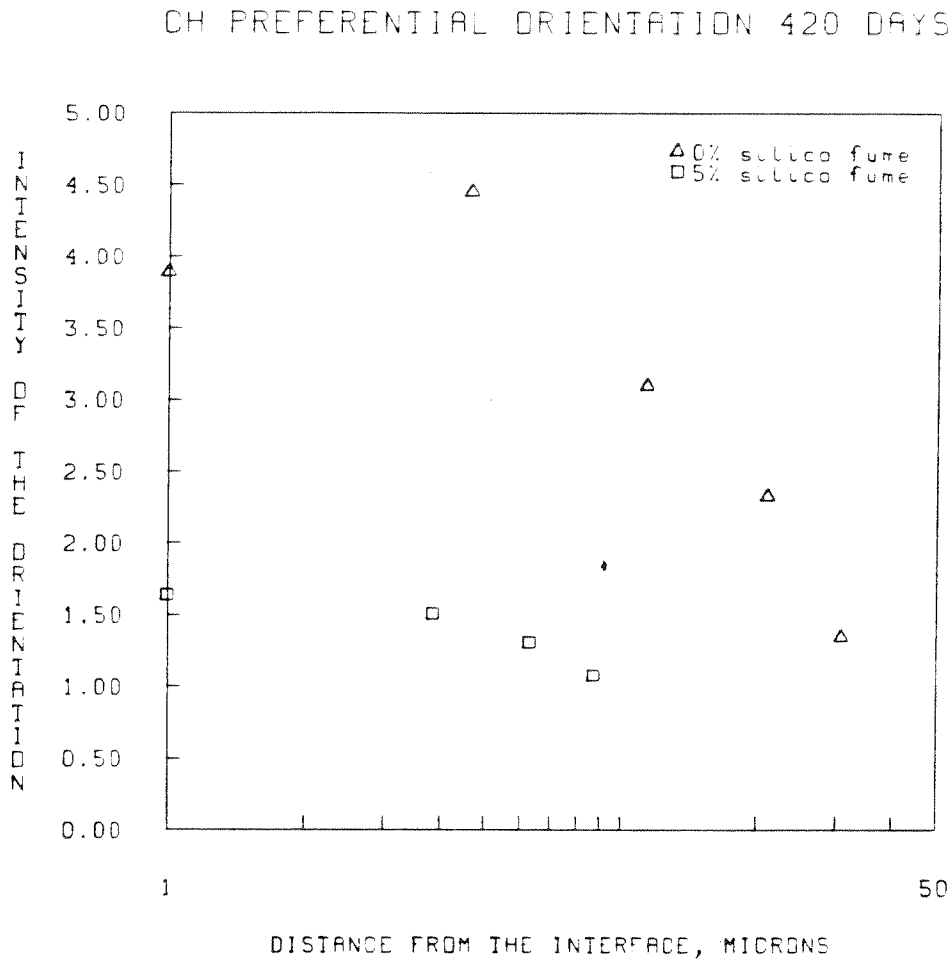

FIG. 23(B). Calcium Hydroxide Preferential Orientation in the Transition Zone

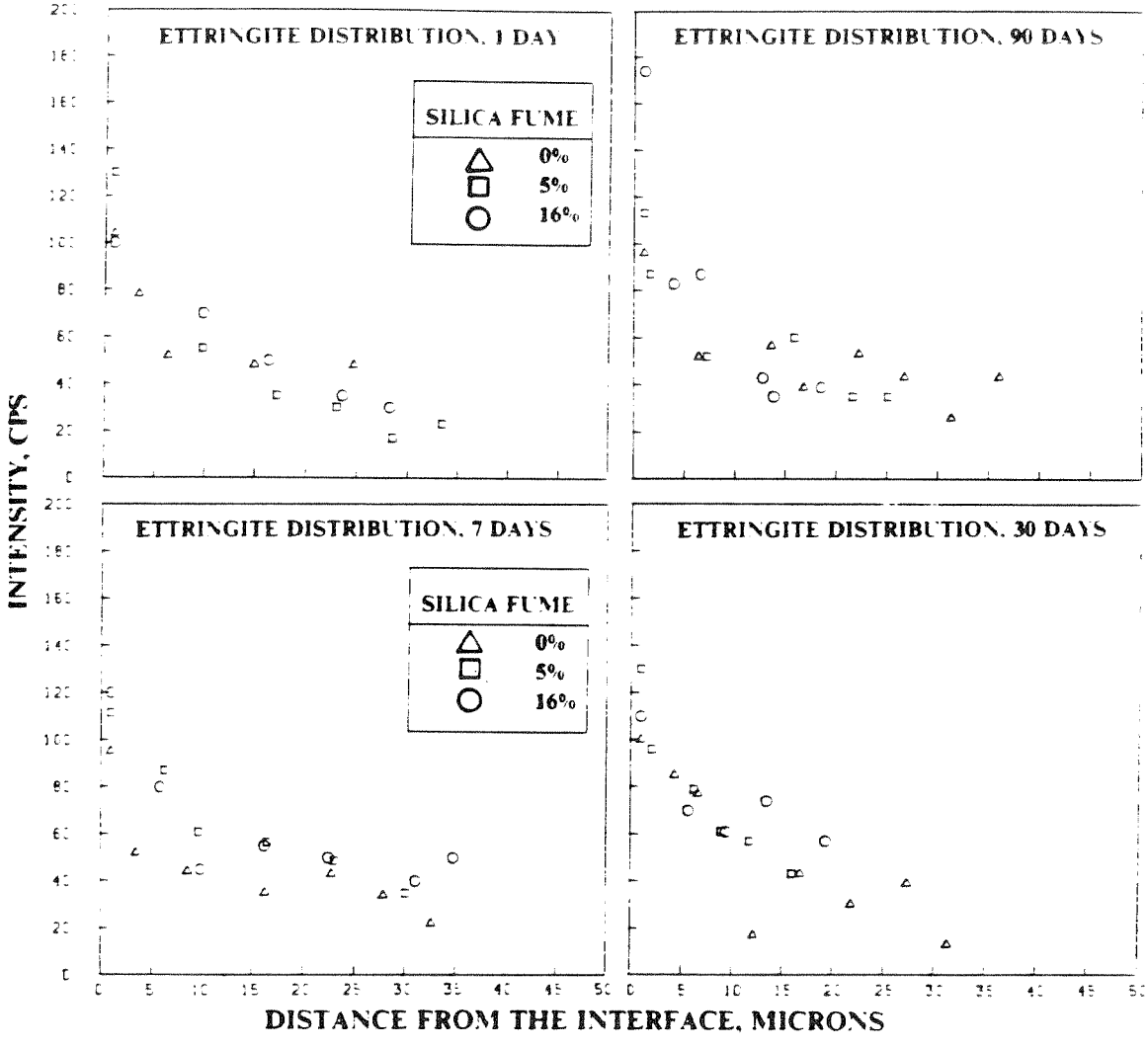

FIG. 24. Ettringite Distribution in the Transition Zone